Wolter Optics for Neutron Transport

Summer internship at the Institut Laue-Langevin under the supervision of Dr Richard Wagner

Niya Petkova

May - August 2022

Contents

Acknowledgements

I would like to thank Dr Richard Wagner for giving me the chance to work on this project, and for his dedicated supervision throughout. It is true that Wolter optics are not rocket science, but they are a useful medium for a second-year student to get a taste of the intricacies and frustrations of academic research. I would further like to extend my gratitude to Prof. Oliver Zimmer, who graciously donated some of his time to teach two interns the basics of nuclear physics, and to Prof. Boris Khaykovich from MIT, who kindly allowed me to look through the early drafts of one of his papers. Finally, I would also like to thank Dr Michael Jentschel for an entertaining tour of the reactor, Giacomo and Vlad for a truly marvellous hike, Valentin for his infinite supply of banana facts, and the other interns in the group: AJ, Sasha, Théo, Clément, Bary and Maxi, without whom there would have been no Bureau des Legendes (with or without additives).

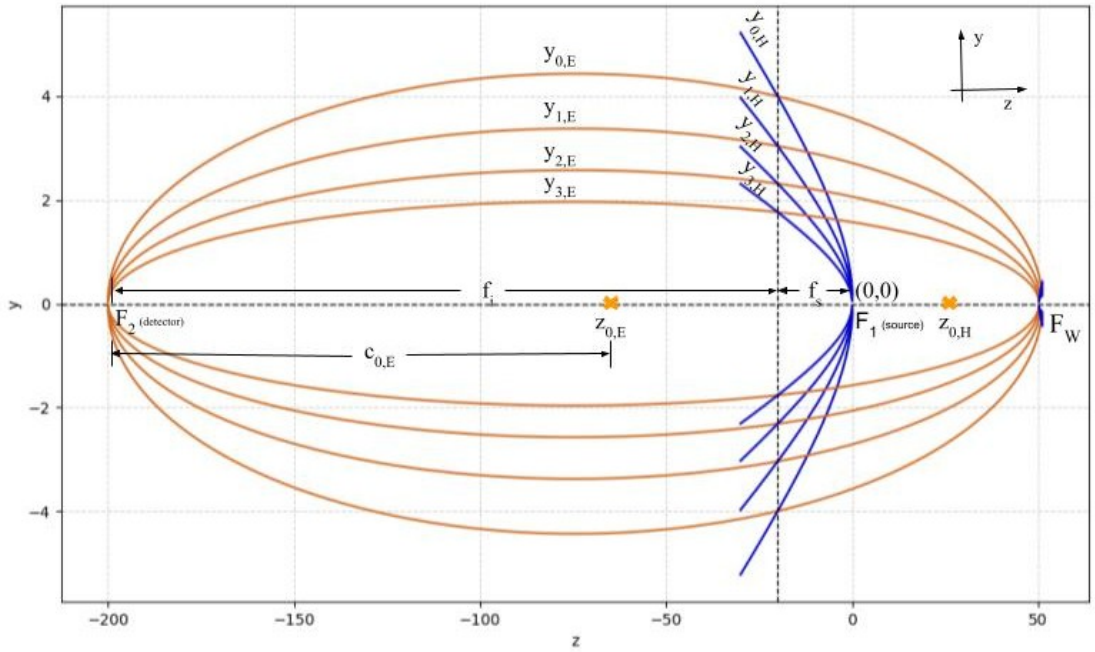

Figure 1: Nested Wolter Optics

1 Preliminaries

This document outlines a method for constructing a system of nested Wolter optics' layers as depicted on Figure 1. A Wolter system consists of an ellipse/a parabola and a hyperbola with one coinciding focus (F_w). There are three possible ways to construct a focusing device like this, the so called Wolter optics of Type I, II and III [1]. Such optical designs have proven useful for the construction of X-ray telescopes and microscopes [1], [2], [3], but here we focus on their possible implementation in the field of neutron transport, and specifically for the NNBAR experiment of the HighNESS project. The proposed optics are of Type I i.e. they provide focusing of a close object to a detector that is further away, functioning like a larger scale microscope [1], [4].

To understand the methodology that follows, it is important to first get acquainted with the geometric layout assumed by this report. The origin of the coordinate system is taken to be the position of the neutron source, which is sitting at the unshared focal point of the outermost hyperbola (F_1 on Figure 1). The neutron detector is placed at the remaining focal point of the outermost ellipse (F_2 on Figure 1). The semi-major axes of the ellipses stretch in the z-direction of the coordinate system to comply with the notation of the neutron ray-tracing program McStas. The semi-minor axes extend into the y-direction. The x-axis goes along the width of the mirrors, which is restricted externally by the parameters of the neutron facility.

The condition that the intersection point of the hyperbolas and the ellipses remains at the same z-coordinate for all nested layers is artificially imposed. Hence, three parameters are constant for all mirrors in the system: the distances f_s and f_i which define the z-position of the hyperbola-ellipse intersection points, and the horizontal length of hyperbolas, L_H, which is taken to be the same for all hyperbolic mirrors.

When a parameter changes between the nested mirrors, a subscript is supplied for each level. For a system of n levels, the subscripts range from 0 to $(n-1)$. The mirrors are numbered from the

outermost layer (index 0) going inwards to levels with larger indices. If a general parameter derivation is discussed, the index n is used to indicate universality of the equations. If the derivation is only applicable to a specific level, then the index of that level is specified.

Here is a list of the notation for all relevant parameters:

- R_n - intersection point of the ellipse and the hyperbola of the nth nested level
- r_n - height of the nth layer of optics at R_n (r_0 given by the set-up of the experiment - maximum allowed height of the optics)
- f_s - z-distance from the source to R_n (constant for all layers)
- f_i - z-distance from R_n to the detector (constant for all layers)
- $f = f_i + f_s$ - z-distance between the source and the detector (constant for all layers)
- L_H - z-length of a hyperbolic section of the optics (constant for all layers, $L_H \leq f_s$)
- $L_{n,E}$ - z-length of an ellipsoid section of the optics (approx. constant for all layers, $L_{n,E} \leq f_i$)
- L_n(or L_{optic}) $= L_H + L_E$ - z-length of the nth Wolter layer
- $b_{n,E}$ and $b_{n,H}$ - semi-minor axes of the nth ellipse and hyperbola
- $a_{n,E}$ and $a_{n,H}$ - semi-major axes of the nth ellipse and hyperbola
- $c_{n,E}$ and $c_{n,H}$ - focal distances of the nth ellipse and hyperbola
- $y_{n,E}$ and $y_{n,H}$ - equations of the nth ellipse and hyperbola
- β_1 - angle between the optical axis and the ray passing from the source to R_0
- β_2 - angle between the optical axis and the ray passing from R_0 to the detector
- m - reflectivity of the mirrors ($m = 6$ is assumed for all simulated mirrors)

Sections 3 and 4 of this report provide a general background for the creation of nested arrays of Wolter optics, while the rest of the document focuses on McStas and the simulations performed for the NNBAR experiment. Section 6 employs the specific parameters for the NNBAR experiment, but the code itself is not restricted to NNBAR. A more detailed introduction to the code is provided in Appendix III.

2 On the NNBAR

The NNBAR is an experiment proposed by the HighNESS project at the ESS. Its purpose is to search for a neutron-antineutron oscillation, which could provide an explanation to the matter-antimatter asymmetry observed in the universe [5], [6]. Such an experiment was previously performed at the ILL without being able to discover the desired oscillation [7]. The aim of the NNBAR is to improve upon this first experimental effort by at least three orders of magnitude [5], [8]. Hence, the unit figure of merit (FOM) is introduced, with FOM = 1 corresponding to the efficiency of the original ILL trial. An improvement of three orders of magnitude would imply FOM = 1000. Since the NNBAR will be running for 3 years, this value can be reduced to $1000/3 \approx 333$ per year. All significant results of FOM > 300 are highlighted in this report.

The FOM value is based on the probability of finding a neutron-antineutron oscillation, which is influenced by two parameters: the number of neutrons reaching the detector (N) and the time of

flight (t) [5]. The latter acquires a larger weighting, as the FOM scales with the square of the time of flight, where t for any given neutron is defined as the time it takes for the particle to reach the detector after its last interaction with the reflector. The set-up of the experiment is very simple; it only consists of a source from which neutrons are guided away via a large beam port opening (LBP), followed either by a nested optical system or a guide to a detector positioned at 200 m away from the source [5]. Since the aim of the optics is to maximize the FOM, it must provide an optimal Nt^2 by guiding as many neutrons to the detector as possible without reducing their time of flight.

A conventional neutron guide might not be the best option, as it would transport many of the neutrons via multiple reflections, thus significantly reducing their time of flight, and absorbing more of the original flux. Thus, it is sensible to look for an optical system that could be placed closer to the source to maximize the time of flight, while focusing the neutrons, so that more of them are accepted by the detector. To construct such a system, we start from the method for building a single-layer Wolter mirror discussed in the following section.

3 Constructing the Top Layer of the System

First, we consider only the outer ellipse and hyperbola (layer 0 on Figure 1), and describe a method for obtaining their equations from the given parameters (f_s, f_i and r_0). Most of these equations for single-layer Wolter optics have already been introduced by Khaykovich et al [9], but the derivation is presented here for completeness.

3.1 Ellipse

An ellipse is defined by the following equations:

$$\frac{(z-h_E)^2}{a_E^2}+\frac{(y_E-k_E)^2}{b_E^2}=1 \tag{1}$$

and

$$a_E^2=c_E^2+b_E^2 \tag{2}$$

where (h_E, k_E) is the position of the center of the ellipse, and z is the coordinate at which y_E is evaluated.

For an ellipse $y_{0,E}$ centered at $(z_{0,E}, 0)$, as on Figure 1, the equations read

$$\frac{(z-z_{0,E})^2}{a_{0,E}^2}+\frac{y_{0,E}^2}{b_{0,E}^2}=1 \tag{3}$$

where we can substitute $z_{0,E}=-(c_{0,E}-2c_{0,H})$. At the intersection of the two mirrors, $z=-f_s$, $y_{0,E}(-f_s)=r_0$, and so

$$\frac{(-f_s+c_{0,E}-2c_{0,H})^2}{a_{0,E}^2}+\frac{r_0^2}{b_{0,E}^2}=1 \tag{4}$$

Rearranging, we get

$$\frac{r_0^2}{b_{0,E}^2}=1-\frac{(-f_s+c_{0,E}-2c_{0,H})^2}{a_{0,E}^2} \tag{5}$$

Hence, the two equations describing an ellipse in the coordinate system of Figure 1 are

$$b_{0,E}^2 = \frac{r_0^2 a_{0,E}^2}{(a_{0,E}^2 - (-f_s + c_{0,E} - 2c_{0,H})^2)} \tag{6}$$

and

$$a_{0,E}^2 = c_{0,E}^2 + b_{0,E}^2 \tag{7}$$

where we can notice that for any given values $c_{0,E}$ and $c_{0,H}$ the system of equations is fully solvable.

3.2 Hyperbola

The two equations defining a hyperbola that opens to the left and is centered at (h_H, k_H) are

$$\frac{(z - h_H)^2}{a_H^2} - \frac{(y_H - k_H)^2}{b_H^2} = 1 \tag{8}$$

and

$$c_H^2 = a_H^2 + b_H^2 \tag{9}$$

The outer hyperbola on Figure 1 is centered at $(z_{0,H}, 0)$ and has the equation

$$\frac{(z - z_{0,H})^2}{a_{0,H}^2} - \frac{y_{0,H}^2}{b_{0,H}^2} = 1 \tag{10}$$

where $z_{0,H} = c_{0,H}$ once again. Evaluating the equations at the intersection point ($z = -f_s$, $y_{0,H}(-f_s) = r_0$):

$$\frac{(-f_s - c_{0,H})^2}{a_{0,H}^2} - \frac{r_0^2}{b_{0,H}^2} = 1 \tag{11}$$

After rearranging, the two equations defining the top hyperbola on Figure 1 become

$$b_{0,H}^2 = \frac{r_0^2 a_{0,H}^2}{(f_s + c_{0,H})^2 - a_{0,H}^2} \tag{12}$$

and

$$a_{0,H}^2 = c_{0,H}^2 - b_{0,H}^2 \tag{13}$$

where, again, it is sufficient to define $c_{0,H}$ in order to solve this system of equations.

3.3 Focal distances of the top ellipse and hyperbola

Equations 6-7 and 12-13 suggest that if one of the parameters of each mirror is known ($a_{0,E}, b_{0,E}$ or $c_{0,E}$ for the ellipse, $a_{0,H}, b_{0,H}$ or $c_{0,H}$ for hyperbola), there will be as many equations as unknowns, so we will be able to define the system. Hence, we try to find the focal distances $c_{0,E}$ and $c_{0,H}$, but to do so we need expressions for some of the angles in the system.

3.3.1 Grazing Angles at Point R_n

Let us call the angles of incidence and reflection from the two mirrors at the point R_0 $\alpha_{0,E}$ and $\alpha_{0,H}$ as on Figure 2. We will now convince ourselves that the angles $\angle LR_0F_w$ and $\angle F_wR_0W$ are also equal to $\alpha_{0,H}$ and $\alpha_{0,E}$, respectively.

As conic sections, hyperbolas inherit the peculiar property that the reflection of a ray incoming from one of their foci appears to be originating from the other focus (proof in Appendix I). Hence, the reflected ray $\overrightarrow{R_0K}$ lies on ray $\overrightarrow{F_wK}$ on Figure 3 and $\angle KR_0F_w$ is a straight angle:

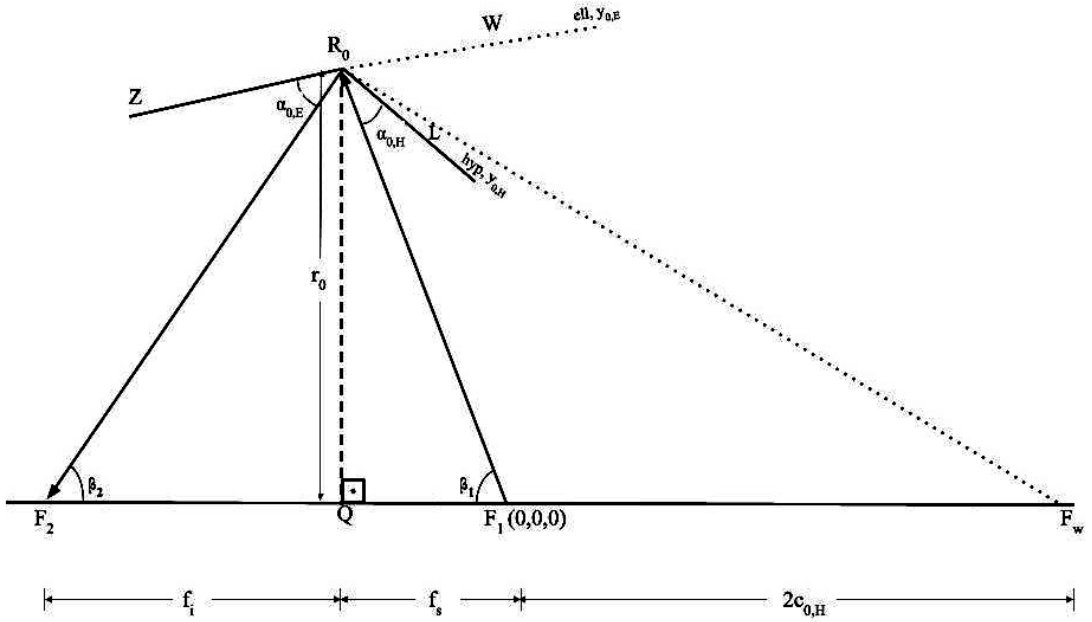

Figure 2: Single Layer Wolter System (figure not to scale)

$$2(90^\circ - \alpha_{0,H}) + \alpha_{0,H} + \angle LR_0F_w = 180^\circ \tag{14}$$

$$180^\circ - \alpha_{0,H} + \angle LR_0F_w = 180^\circ \tag{15}$$

And so

$$\angle LR_0F_w = \alpha_{0,H} \tag{16}$$

As another subset of conic sections, ellipses are defined as the locus of points for which the sum of distances to each of the foci is preserved. To satisfy this condition, a ray passing through one of the foci and incident on any point on the surface of the ellipse has to reflect back to the other focus (proof in Appendix 1). Hence, ray $\overrightarrow{R_0F_2}$ on Figure 4 must be a reflection of ray $\overrightarrow{F_wR_0}$.

Thus, by the law of reflection:

$$\angle F_2R_0Z = \angle F_wR_0W = \alpha_{0,E} \tag{17}$$

So angles $\angle LR_0F_w$ and $\angle F_wR_0W$ on Figure 2 are indeed the same as the angles of reflection from the hyperbola and the ellipse, respectively. We now use this fact to test one peculiar angle property of Wolter optics.

From triangle $F_1R_0F_w$ on Figure 2 we have

$$(180^\circ - \beta_1) + 2\alpha_{0,H} + \angle F_1F_wR_0 = 180^\circ \tag{18}$$

$$\angle F_1F_wR_0 = \beta_1 - 2\alpha_{0,H} \tag{19}$$

Taking the tangent of this angle in triangle QR_0F_w, we get

$$tan(\beta_1 - 2\alpha_{0,H}) = \frac{r_0}{f_s + 2c_{0,H}} \tag{20}$$

From this we derive an expression for the angle $\alpha_{0,H}$:

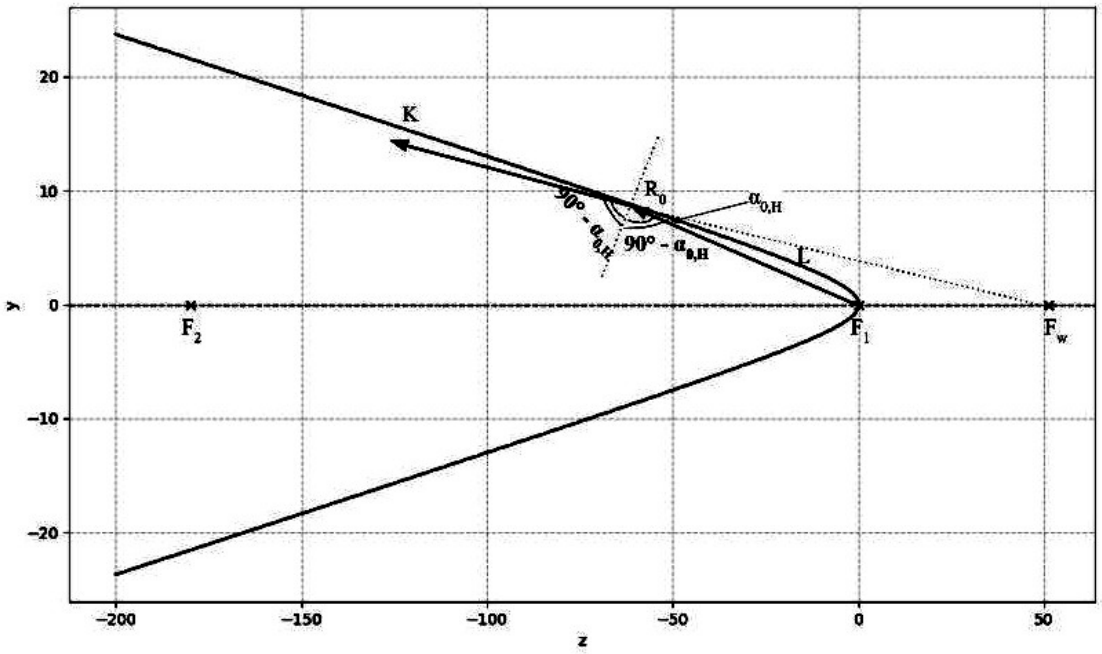

Figure 3: Reflection by a Hyperbola

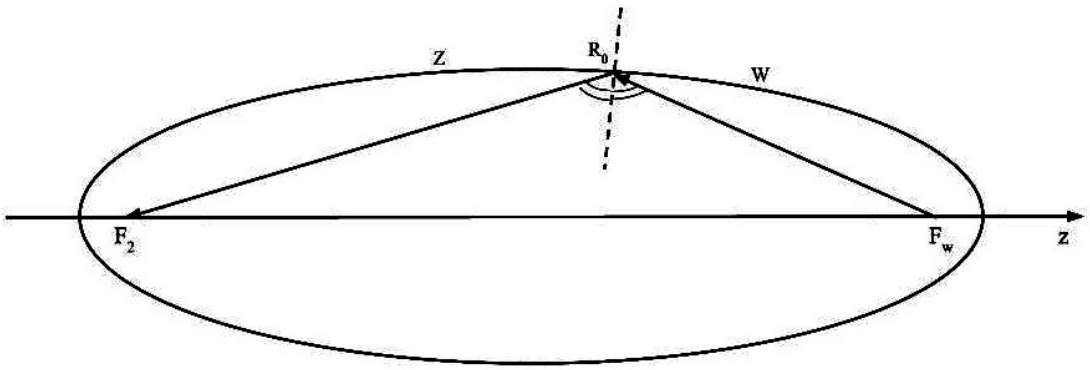

Figure 4: Reflection by an Ellipse

$$\alpha_{0,H} = \frac{\beta_1 - arctan(\frac{r_0}{f_s+2c_{0,H}})}{2} \tag{21}$$

Looking at the external angles to the triangle $F_2R_0F_1$, we also have

$$\beta_1 + \beta_2 = 2(\alpha_{0,E} + \alpha_{0,H}) \tag{22}$$

$$\alpha_{0,E} = \frac{\beta_1 + \beta_2}{2} - \alpha_{0,H} \tag{23}$$

The angles β_1 and β_2 can be found from the dimensions of triangles QR_0F_1 and QR_0F_2:

$$tan(\beta_1) = \frac{r_0}{f_s} \rightarrow \beta_1 = \arctan(\frac{r_0}{f_s}) \tag{24}$$

$$tan(\beta_2) = \frac{r_0}{f_i} \rightarrow \beta_2 = \arctan(\frac{r_0}{f_i}) \tag{25}$$

Substituting into equations 21 and 23:

$$\alpha_{0,H} = \frac{\arctan(\frac{r_0}{f_s}) - \arctan(\frac{r_0}{f_s+2c_{0,H}})}{2} \tag{26}$$

and

$$\alpha_{0,E} = \frac{\arctan(\frac{r_0}{f_s}) + \arctan(\frac{r_0}{f_i})}{2} - \alpha_{0,H} \tag{27}$$

For the particular application of neutron transport, these angles must be very small, as neutron reflections occur only at tiny glancing angles (for nickel and m = 1, $\theta_{critical} = 0.0173\lambda$ rad) [10]. To maximize the number of neutrons that are transported by the system, Khaykovich et al and Bagdasarova [9], [11] assume that the glancing angles at both surfaces are equal. This condition is tested by plotting the angles $\alpha_{0,H}$ and $\alpha_{0,E}$ for a range of different values of $c_{0,H}$ on Figure 5. For the other parameters of the system, the dimensions of the NNBAR experiment are used: $r_0 = 2$ m, $f_i = 180$ m, $f_s = 20$ m.

As the plot shows, the angles differ significantly for most focal distances of the hyperbola, so the condition that they are equal is not inherent in a Wolter system. It is possible that an asymmetric Wolter arrangement where one of the mirrors is able to reflect more neutrons than the other turn out to have some advantages over the symmetric ones, but they will not be the focus of this narrative. Instead, the upcoming section aims to derive an expression for $c_{0,H}$ that returns the value of 12.5 m characteristic of the symmetric NNBAR system on Figure 5.

3.3.2 Focal distances $c_{0,E}$ and $c_{0,H}$

Assuming that the two glancing angles are equal $\alpha_{0,E} = \alpha_{0,H} = \theta_0$, their value can be derived from equations 24-25:

$$\theta_0 = \frac{\beta_1 + \beta_2}{4} = \frac{1}{4}(\arctan(\frac{r_0}{f_i}) + \arctan(\frac{r_0}{f_s})) \tag{28}$$

With this definition of θ_0, the focal distances of the top ellipse and hyperbola can now be derived from equation (20) as follows:

$$c_{0,H} = \frac{1}{2}\left[\frac{r_0}{\tan(\beta_1 - 2\theta_0)} - f_s\right] \tag{29}$$

Inserting the parameters of the NNBAR, the expression results exactly in the value given by the equal angles assumption on Figure 5.

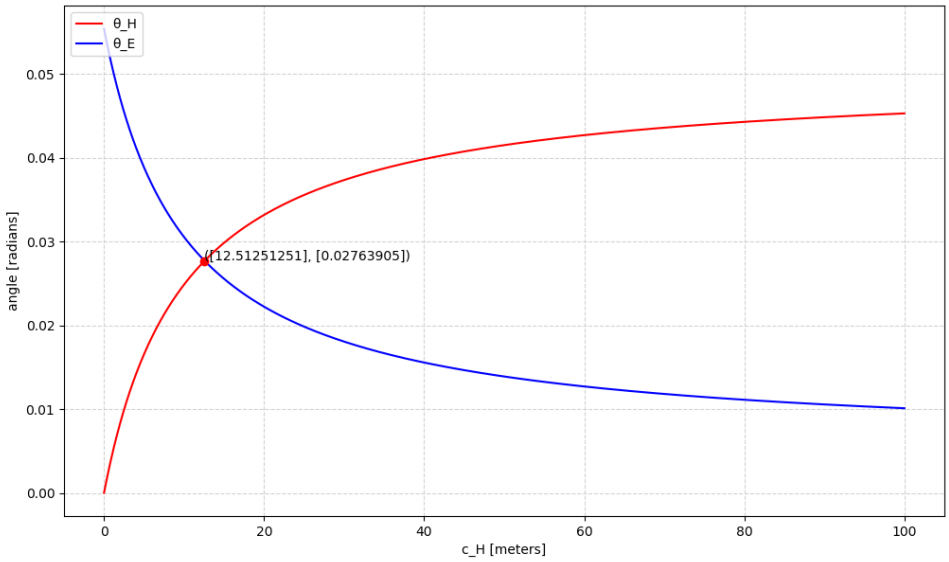

Figure 5: Grazing angles at intersection point for different values of c_H

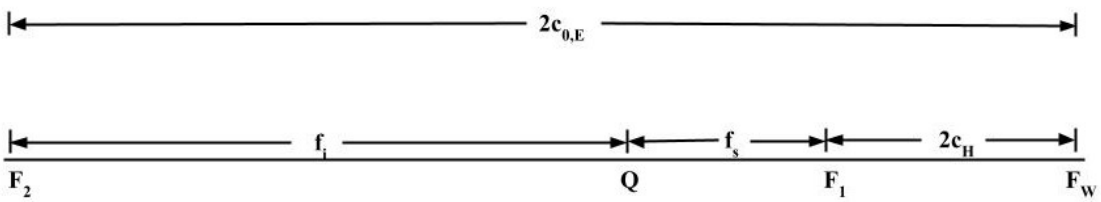

Figure 6: Parameters of the Wolter system

An expression for the focal distance of the ellipse is similarly derived by relating $c_{0,E}$ to the values of f_s, f_i and $c_{0,H}$ as on Figure 6:

$$2c_{0,E} = f_i + f_s + 2c_{0,H} \tag{30}$$

$$c_{0,E} = c_{0,H} + \frac{f_s + f_i}{2} \tag{31}$$

3.4 Solving for the parameters of the top ellipse

We use the above equations to define a general expression for each of the parameters of the ellipse ($a_{0,E}, b_{0,E}$ and $c_{0,E}$) from the givens (f_i, f_s, r_0).

Starting from equation 6:

$$b_{0,E}^2 = \frac{r_0^2 a_{0,E}^2}{(a_{0,E}^2 - L^2)} \tag{32}$$

where $L = -f_s + c_{0,E} - 2c_{0,H}$.

Substituting $b_{0,E}^2 = a_{0,E}^2 - c_{0,E}^2$:

$$a_{0,E}^2 - c_{0,E}^2 = \frac{r_0^2 a_{0,E}^2}{a_{0,E}^2 - L^2} \tag{33}$$

Noting the condition $a_{0,E}^2 \neq L^2$, we have:

$$r_0^2 a_{0,E}^2 + (-a_{0,E}^2 + c_{0,E}^2)(a_{0,E}^2 - L^2) = 0 \tag{34}$$

This simplifies to the equation

$$a_{0,E}^4 - a_{0,E}^2(L^2 + c_{0,E}^2 + r_0^2) + c_{0,E}^2 L^2 = 0 \tag{35}$$

which has roots

$$a_{0,E}^2 = \frac{(L^2 + c_{0,E}^2 + r_0^2) \ \pm \ \sqrt{(L^2 + c_{0,E}^2 + r_0^2)^2 - 4c_{0,E}^2 L^2}}{2} \tag{36}$$

To have a well-defined semi-minor axis, b_E, we take the higher value. Hence, the ellipse has a semi-major axis

$$a_{0,E} = \left[\frac{(L^2 + c_{0,E}^2 + r_0^2) \ + \ \sqrt{(L^2 + c_{0,E}^2 + r_0^2)^2 - 4c_{0,E}^2 L^2}}{2} \right]^{\frac{1}{2}} \tag{37}$$

where $L = (-f_s + c_{0,E} - 2c_{0,H})$ and $c_{0,E}$ is expressed from equations 29 and 31 as

$$c_{0,E} = \frac{f_s + f_i}{2} + \frac{1}{2}\left[\frac{r_0}{\tan(\beta_1 - 2\theta_0)} - f_s \right] \tag{38}$$

with θ_0 given by equation 28.

Equations 37 and 38 fully define $a_{0,E}$ and $c_{0,E}$, so we can use equation 7, $b_{0,E}^2 = a_{0,E}^2 - c_{0,E}^2$, to find $b_{0,E}$ and complete the mathematical description of the top ellipse.

3.5 Solving for the parameters of the top hyperbola

Similarly, we now define the parameters of the hyperbola ($a_{0,H}, b_{0,H}$ and $c_{0,H}$) in terms of the givens (f_s, f_i, r_0).

Starting from equation 12

$$b_{0,H}^2 = \frac{r_0^2 a_{0,H}^2}{(f_s + c_{0,H})^2 - a_{0,H}^2} \tag{39}$$

and substituting $b_{0,H}^2 = c_{0,H}^2 - a_{0,H}^2$:

$$c_{0,H}^2 - a_{0,H}^2 = \frac{r_0^2 a_{0,H}^2}{(f_s + c_{0,H})^2 - a_{0,H}^2} \tag{40}$$

Noting the condition $a_{0,H}^2 \neq (f_s + c_{0,H})^2$:

$$(c_{0,H}^2 - a_{0,H}^2)((f_s + c_{0,H})^2 - a_{0,H}^2) = r_0^2 a_{0,H}^2 \tag{41}$$

This simplifies to the quadratic equation

$$a_{0,H}^4 - a_{0,H}^2 N + c_{0,H}^2 (f_s + c_{0,H})^2 = 0 \tag{42}$$

where

$$N = c_{0,H}^2 + (f_s + c_{0,H})^2 + r_0^2 \tag{43}$$

This has roots

$$a_{0,H}^2 = \frac{N \ \pm \ \sqrt{N^2 - 4c_{0,H}^2 (f_s + c_{0,H})^2}}{2} \tag{44}$$

We take the lower value (empirically tested with Khaykovich et al. data).

Hence the hyperbola has a major axis of length

$$a_{0,H} = \left[\frac{N \ - \ \sqrt{N^2 - 4c_{0,H}^2 (f_s + c_{0,H})^2}}{2} \right]^{\frac{1}{2}} \tag{45}$$

where $N = c_{0,H}^2 + (f_s + c_{0,H})^2 + r_0^2$ and $c_{0,H}$ is defined by equations 29 and 31.

Equation 45 fully defines $a_{0,H}$, so we can use equation 9 ($b_{0,H}^2 = c_{0,H}^2 - a_{0,H}^2$) to find $b_{0,H}$ and construct the top hyperbola.

4 Nesting Layers of Wolter Optics

Following similar considerations as in the previous section, the formulas there can be extended to any layer of the nested system. For the n-th hyperbola, equations 45 and 29 can be generalized as follows

$$a_{n,H} = \left[\frac{N \ - \ \sqrt{N^2 - 4c_{n,H}^2 (f_s + c_{n,H})^2}}{2} \right]^{\frac{1}{2}} \tag{46}$$

where $N = c_{n,H}^2 + (f_s + c_{n,H})^2 + r_n^2$ and $c_{n,H}$ is defined as

$$c_{n,H} = \frac{f_s \theta_n}{(\frac{r_n}{f_s} - 2\theta_n)} \tag{47}$$

with

$$\theta_n = \frac{1}{4}(arctan(\frac{r_n}{f_i}) + arctan(\frac{r_n}{f_s})) \tag{48}$$

Equation 8 can also be generalized to produce the height of any nested hyperbola at a given point z:

$$y_{n,H} = b_{n,H}\sqrt{\frac{(z - c_{n,H})^2}{a_{n,H}^2} - 1} \tag{49}$$

Similarly, for the n-th ellipse, equations 37 and 38 become:

$$a_{n,E} = \left[\frac{(L^2 + c_{n,E}^2 + r_n^2) \; + \; \sqrt{(L^2 + c_{n,E}^2 + r_n^2)^2 - 4c_{n,E}^2 L^2}}{2}\right]^{\frac{1}{2}} \tag{50}$$

where $L = (-f_s + c_{n,E} - 2c_{n,H})$ and

$$c_{n,E} = c_{n,H} + \frac{f_s + f_i}{2} \tag{51}$$

while the height of the ellipse (equation 4) at a given point along the z-axis is now given by

$$y_{n,E}(z) = b_{n,E}\sqrt{1 - \frac{(z + c_{n,E} - 2c_{n,H})^2}{a_{n,E}^2}} \tag{52}$$

Notice that in these equations the only unknown is the height r_n at the intersection point of the n-th ellipse and the n-th hyperbola, so the only thing that is left to define is an algorithm for transitioning from the top height r_0 to the r_n of the nested layers.

4.1 Arrays of r_n Heights

Firstly, we apply two conditions to our optical construction that will optimize the neutron transport it can provide. These conditions will be used to transition between any two consecutive layers of the system.

To begin with, we want the ray reflecting off the edge of the upper layer in Figure 7 (ray 1), to reach the other edge of the layer, so that it does not get lost by the system. Then we also require that the ray that gets reflected at R_n by the upper layer (ray 2) passes just over the surface of the nested hyperbola, so that all rays at higher glancing angles get collected by the bottom mirror.

The first condition could in principle be used to define an appropriate length L_E of the ellipse for any given starting parameters of the system. The author of the document apologizes for not having the time to do that.

The second condition allows us to derive the following equation:

$$tan(\beta_n) = \frac{y_{n-1,H}(L_H - f_s)}{f_s - L_H} = \frac{r_n}{f_s} \tag{53}$$

$$y_{n-1,H}(L_H - f_s) = r_n \frac{(f_s - L_H)}{f_s} \tag{54}$$

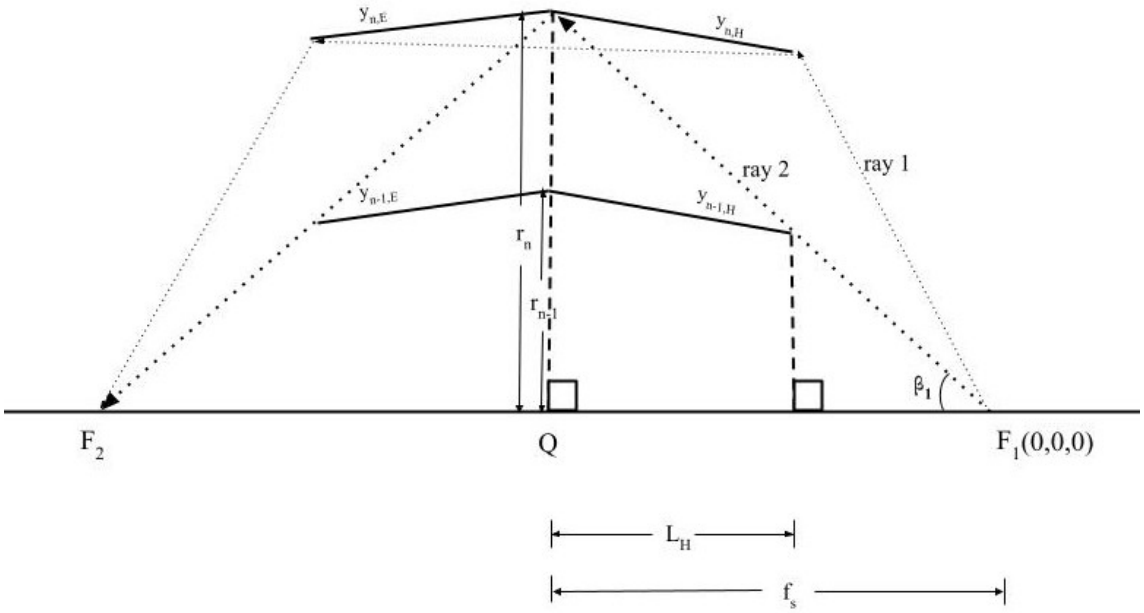

Figure 7: Conditions for Nesting Wolter Optics

Now, a little trick discovered empirically can be applied. We assume (validity checks will follow) that

$$\frac{y_{n-1,H}(L_H - f_s)}{y_{n,H}(L_H - f_s)} = \frac{r_{n-1}}{r_n} \tag{55}$$

So

$$y_{n-1,H}(L_H - f_s) = \frac{r_{n-1}}{r_n} y_{n,H}(L_H - f_s) \tag{56}$$

Substituting this back into the previous equation:

$$\frac{r_{n-1}}{r_n} y_{n,H}(L_H - f_s) = r_n \frac{(f_s - L_H)}{f_s} \tag{57}$$

We arrive at an expression for r_{n-1}:

$$r_{n-1} = (r_n)^2 \frac{(f_s - L_H)}{f_s y_{n,H}(L_H - f_s)} \tag{58}$$

Now, this expression is used to test the assumption that it emerged from. On Figure 8, we plot

$$\frac{y_{n-1,H}(z)}{y_{n,H}(z)} - \frac{r_{n-1}}{r_n} \tag{59}$$

for z values covering the range from the start of the optics (z = 0) to the detector (z = -f). The y-values are calculated using the appropriate heights and equations 49-52 and 12.

The top plot shows that the approximation is very good for any sufficiently small coordinates z $z < -5$ m. For such z, the difference between the two ratios is less than 0.004 at its extreme. The approximation works worst for the top layer, and improves as going deeper into the nested mirror arrangement. For the innermost layer ($n = 6$, $(n-1) = 5$) the maximum deviation of in the region of $z < -5$ m is 0.0004. However, looking at the bottom plot on Figure 8, it can be seen

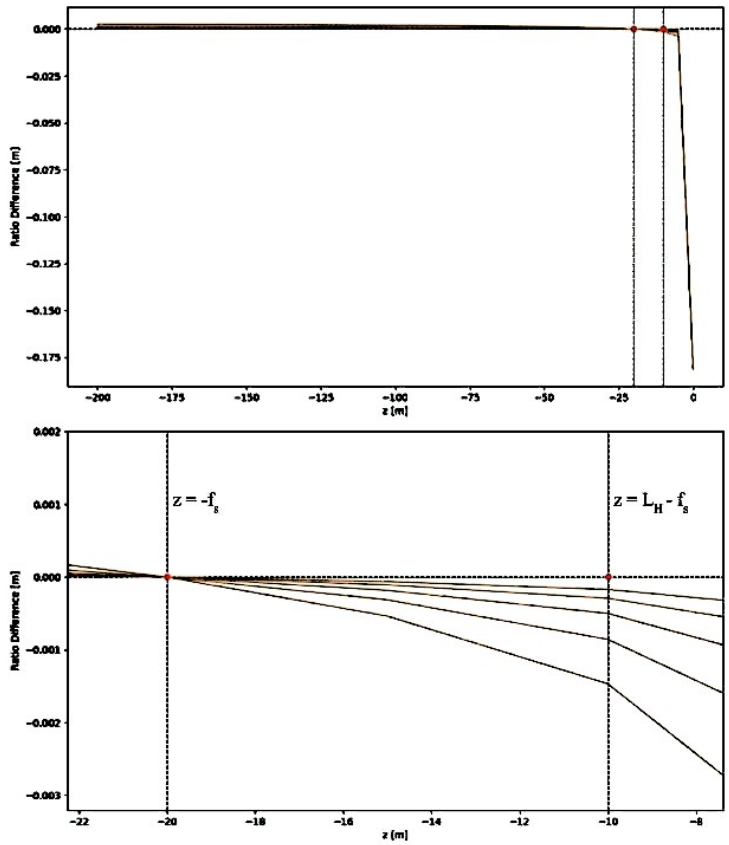

Figure 8: Differences between ratios $\frac{y_{n-1,H}(z)}{y_{n,H}(z)}$ and $\frac{r_{n-1}}{r_n}$ for different z-values of a system of six nested levels with a zoom-in into regions around $z = -f_s$ and $z = L_H - f_s$. The top line on the left corresponds to the difference for levels $n = 0$ and $n = 1$.

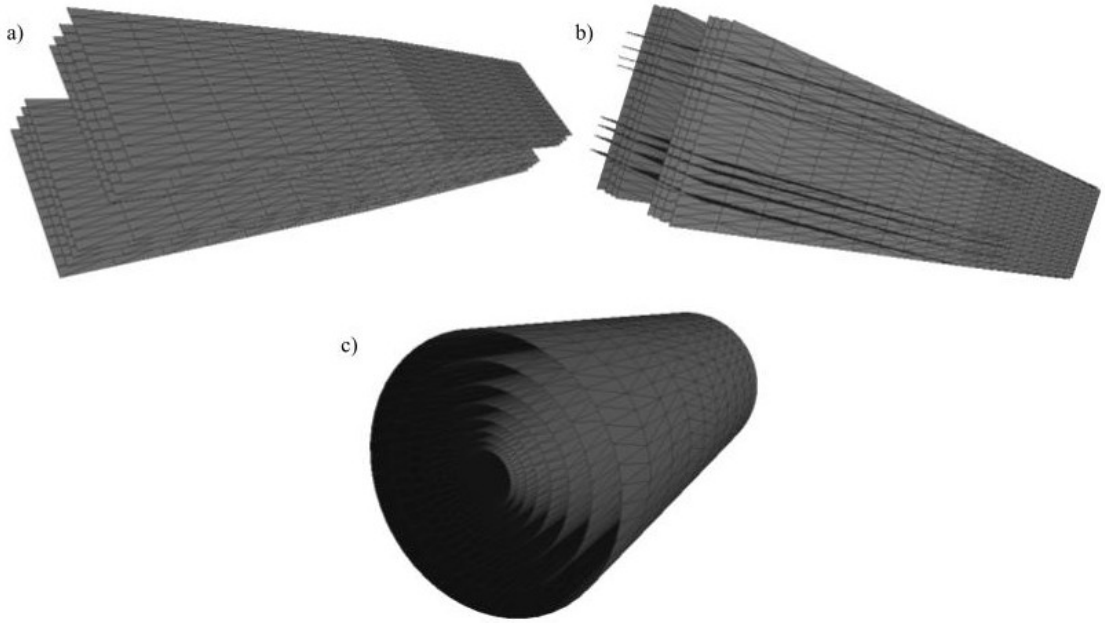

Figure 9: a) Monoplanar, b) Double planar, c) Toroidal (Hypothetical, not created)

that at the relevant z-coordinate z = $L_H - f_s$ the maximum difference for the two uppermost layers is 0.0014. This drops to 0.0002 for $n = 6$ ($(n-1) = 5$ curve). Rounding errors are negligible as the lower plot shows an almost perfect match of all layers at the intersection points R_n, where indeed, we would expect that $\frac{r_{n-1}}{r_n} = \frac{y_{n-1,H}(-f_s)}{y_{n,H}(-f_s)}$ as $y_{n-1,H}(-f_s) = r_{n-1}$ and $y_{n,H}(-f_s) = r_{n-1}$. Hence, the approximation holds for the purposes of the following simulations, and equation 55 is a valid assumption. (As an aside, a similar argument is provided in Appendix 2 for the ellipses.)

Equation 55 can now be used recursively to define an array of intersection heights which can be plugged back into equations 49-52 to calculate the parameters of each consecutive layer of optical system.

4.2 Arrays of Semi-minor Axes ($b_{n,E}$ and $b_{n,H}$)

The semi-minor axes of the ellipses and the hyperbolas can be found from equations 49-52, 2 and 9, and an algorithm to do that is provided in the code implementation of this project. For engineering purposes, it is important to control that the spacing between consecutive layers does not get too small. This has unfortunately not yet been integrated into the code, so users are adviced not forget to check this condition manually.

5 Algorithm for Creating Wolter Optics for McStas

Having considered the mathematical description of nested multi-layer Wolter optics, we must now turn to optimising their parameters for the purposes of the NNBAR experiment. The McStas neutron simulation environment provides the instrument component Guide anyshape, which allows for an OFF file with the dimensions of a specific guide or optical system to be imported. We consider three types of set-ups of nested Wolter optics: monoplanar, double planar and toroidal (Figure 9 a), b) and c) respectively) [12].

To construct these optics, an algorithm for creating OFF files is required. The OFF file format begins with a line reporting the number of vertices, faces and edges (the last can be left as 0) that have to be constructed. After that the file lists the coordinates of each of the vertices in some set order, followed by lines connecting these coordinates into faces. In order to encode monoplanar optics in OFF files, we separate each mirror into rectangles and record them as the faces. Firstly, the range covered by the optics going around the z-axis is splitting into some finite input number of segments. Then, the intersection heights, r_n, for each nested level are calculated via equation 55. For each of these heights (so for each nested levels, the y-coordinates of each z-segment endpoint are derived via equations 49-52. Both negative and the positive y-values are taken into account, as they represent the two mirrors below and above the optical axis. Finally, the x-axis could also be split into segments and for each of those, the x and y coordinates of each point along the z-axis could be calculated. It is also possible, and easier for simulations to handle, to skip this last step and consider each big panel along the entirety of the used x-coordinates as one face. Afterwards, this method is repeated for all of the other nested levels. The algorithm relies on setting a specific order of appearance of the coordinates in the OFF file, so that they can be more easily connected into faces by the appropriate code (see Appendix III for details).

Once monoplanar optics are created, a second pair of them can be produced and rotated by 90 degrees to get a double planar arrangement. The same algorithm as before can be used to produce a second monoplanar optic but its x and y coordinates are exchanged in order to perform the rotation.

Finally, toroidal optics are a proposed geometry in which the mirrors fully encircle the beam. A big advantage of these optics for the NNBAR experiment is the reduction of the number of reflections: a toroidal geometry requires a single reflection by each of its hyperbolic and elliptical sections to change both the x and the y components of a neutron's velocity (in contrast with the 4 reflections (2 per plane) required by double planar optics). Since toroidal optics could transport neutrons with less reflections, less neutrons will be lost during the interactions with the mirrors. The m value of the mirrors will determine the exact absorption rate but, as an example, if the probability of absorption is 20 percent, toroidal optics will transport 0.8 x 0.8 N = 0.64 N out of N neutrons, and for double planar mirrors, the flux will be reduced to 0.8 x 0.8 x 0.8 x 0.8 = 0.41 of the original one. Hence, toroidal optics are likely to be much more efficient then planar ones for the purposes of the NNBAR.

However, this geometry does not come without disadvantages - a toroidal set-up needs to be constructed out of a multitude of tiny elements assembled into a continuum of hyperbolic and elliptical sections, which is a much harder (and more expensive) procedure than the "simple" joining of two-mirrors for a planar arrangement. It might therefore be useful to consider other regular polygons, such as hexagons or octagons of Wolter optics as the middle ground between planar and toroidal set-ups. For many of the incoming particles, such designs will provide focusing with only two reflections, although a fraction of the neutrons will still undergo the full 4 reflections.

6 Simulation Results

The arrangement of the NNBAR experiment fixes two of the important parameters for the construction of the optical system - the maximum height $r_0 = 2$ m and the combined focal length, f, which is equivalent to the 200 meter length of the proposed beamline [5]. In addition, the set-up of the experiment is such that to prevent radiation leakage, two concrete blocks have been placed - a 'monolith' at 5.5 m, and a 'bunker' 15 m away from the source [5]. Whether any optics could be inserted in between would depend on the ability of their constituent materials to endure radiation and heat exposure. If the positioning of mirrors there is to prove impossible, that would result in a lower limit to the distance between the source and the optics. If not, then

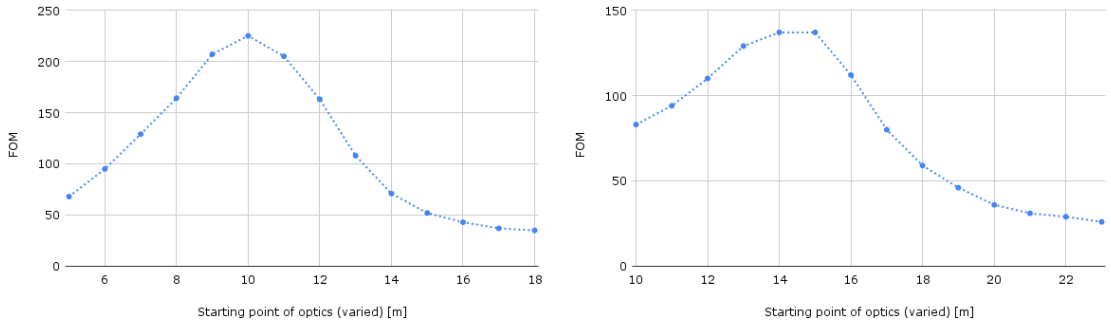

(a) $L = 40$ m, $L_H = 15$ m, $f_s = 25$ m, $n = 8$, starting point by design: 10 m

(b) $L = 40$ m, $L_H = 10$ m, $f_s = 25$ m, $n = 8$, starting point by design: 15 m

Figure 10: Variation in FOM value for two optics that are placed at different starting positions

the minimum distance would be the combined 5.5 meter length of the source and the large beam port (LBP).

Different set-ups within and outwith the boundaries of the monolith and bunker walls are tested here and some trends in the obtained FOM values are highlighted. Four parameters are varied in the system - the number of nested levels, n, the length of the hyperbolic section L_H of the optics, the total length L, which defines the elliptical portion of the optics, and the distance from the source to the mirrors, f_s. But before we can look at the effect of the number of nested mirrors on the figure of merit, we first need to discuss one more inherent property of the Wolter systems.

6.1 Position of Optics

It is important to remember that Wolter optics are only constructed for a specific position, as their hyperbolic sections have to begin at the z-coordinate $f_s - L_H$. To illustrate this point, the starting position od two separate 8-layers optical systems is varied along the z-axis on Figure 10. On part a) of that figure, $L = 40$ m, $L_H = 15$ m, $f_s = 25$ m. Hence, the optics is designed to be positioned at the z-coordinate $f_s - L_H = 25 - 15 = 10$ m. Indeed, if the OFF file of this optics is consulted, it will display 10.0 as its first z-coordinate. We can vary externally its position in the simulation by setting the optics at different coordinates in McStas. The results on Figure 10 a) show that the peak in FOM value is exactly at the designed starting point of the optics (10 m), which appears when the McStas component for the optics is set to z = 0. Deviating from this position leads to a decrease in the FOM, as the optics gets worse at focusing the neutron beam.

On Figure 10 b), the parameters $L = 40$ m, $L_H = 10$ m and $f_s = 25$ m are selected. Hence, the optics is designed to have its hyperbolic section starting at z = $f_s - L_H = 15$ m. Indeed, as before, we can see that the FOM values on Figure 10 b) peak around the starting point of 15 m, and there is a sharp decline in FOM as the optics position sways away from the optimum. Comparing the two simulations, it seems that optics with larger L_H (Figure 10 a)), are better tuned to be placed further away from the source than their designated positions, while optics with smaller L_H (Figure 10 b)) perform much worse even if their starting point is only slightly varied. We will soon see that the mirror system in a) has a ratio $\frac{L_H}{L}$ that is closer to $\frac{1}{3}$ than that of the second optics, so its L_E length must be more appropriate to the chosen L_H length. Hence, the first system is a better approximation to the desired optimal Wolter optics of length L = 40 m, and is more efficient than the second one. In both cases however, it is important to remember that the starting position of the optics is integrated into its design, and the performance of the mirrors can only get worse if that point is varied. For this reason, in all simulations that follow, the optics are placed only at their designated positions.

	FOM					
n [levels]	case 0: L_H = 10, L = 50, f_s = 20, start of optics: 10	case 1: L_H = 10, L = 40, f_s = 20, start of optics: 10	case 2: L_H = 20, L = 40, f_s = 30, start of optics: 10	case 3: L_H = 15, L = 30, f_s = 25, start of optics: 10	case 4: L_H = 10, L = 20, f_s = 20, start of optics: 10	case 5: L_H = 5, L = 10, f_s = 15, start of optics: 10
1	35	33	29	24	19	12
2	60	61	55	43	34	19
3	83	86	82	66	51	27
4	110	114	109	91	68	38
5	143	142	133	115	90	50
6	174	172	141	134	106	62
7	198	200	142	148	127	75
8	214	215	141	154	142	87
9	225	230	138	156	159	99
10	230	237	136	155	169	111
11	232	240	135	154	174	122
12	230	240	134	151	175	133
13	227	239	133	151	176	145
14						155
15						166
16						175
17						184
18						190
19						197
20						202
21						204

Figure 11: Raw data: FOM variation with different number n of nested mirrors for 4 Wolter optical systems

6.2 Varying n

The FOM for four different optics with the parameters described on Figure 12 are now run for systems with different number of layers n (keeping L_H, L and f_s constant). All of the optics in this simulation are symmetric, having equal lengths L_E and L_H of their elliptical and hyperbolic sections. The raw data in Figure 11 shows that all of the optics eventually reach a plateau in their FOM values, and after that the addition of further nested mirrors to the system does not significantly improve the figure of merit, or in some cases (blue curve on Figure 12), it might even lead to a slight decrease in efficiency.

When the data from the symmetric optics on Figure 11 is plotted on Figure 12, the FOM plateau is not visible for the shortest optic, as it lies outwith the selected range of n values. The optics experience a shift in their FOM saturation point toward a larger value n of nested levels, as the total lengths L get shorter. It also appears that the longer optics can not produce a figure of merit that is equivalent to the ones given by the shorter optics. This might be because the increase in the length of the optics leads to a decrease in the time of flight after the reflection of the neutron. At some point the decrease in t outweighs the increase in the transported flux due to the larger acceptance of the longer mirrors. It is not necessary however that this optimal length is already reached at L = 10 m, as Figure 12 suggests. All optics that are plotted on that figure are symmetric, and therefore do not have L_E controlled in such a way that the optimal ratio $\frac{L_E}{L_H}$ is reached. This ratio will be discussed more in section 6.4, but it is a possible explanation to the decrease in FOM that we observe as L gets larger.

A similar simulation is now performed with asymmetric optics of $L_H = 10$ m, $f_s = 20$ m, and L of 40 and 50 m. In contrast to Figure 12, the data on Figure 13 shows that there is no significant decrease in the maximum attainable FOM value as L increases. It is therefore, complicated to predict the optimal length L of the optics, but, as before, the plot shows a clear plateauing of the FOM value as some critical number n_c of nested mirrors is reached. The optimal n_c varies

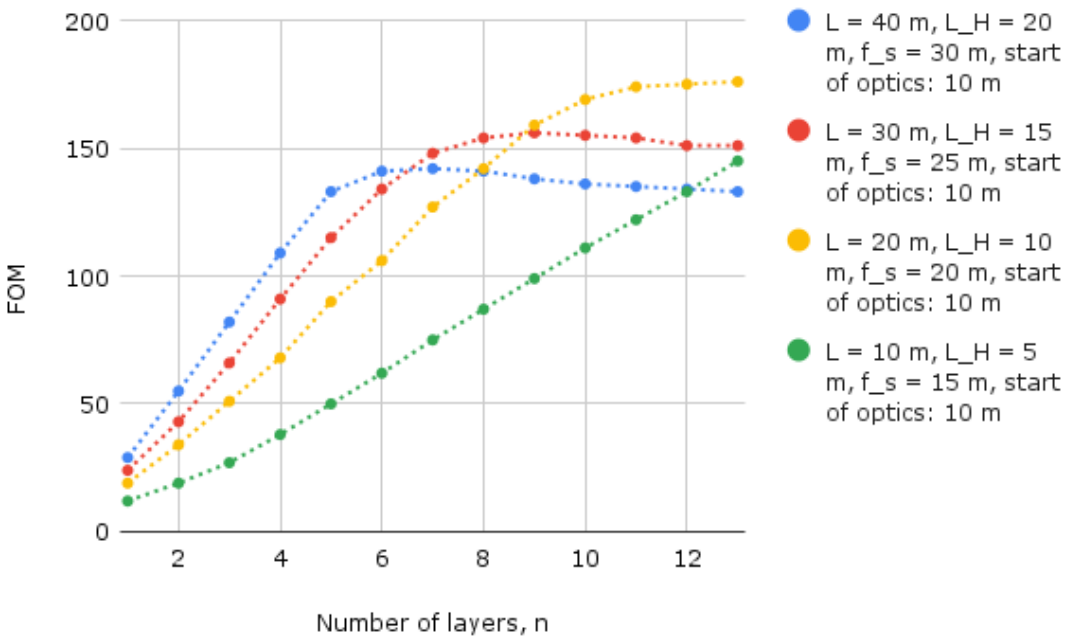

Figure 12: FOM variation with different number n of nested mirrors for 4 symmetric Wolter optical systems

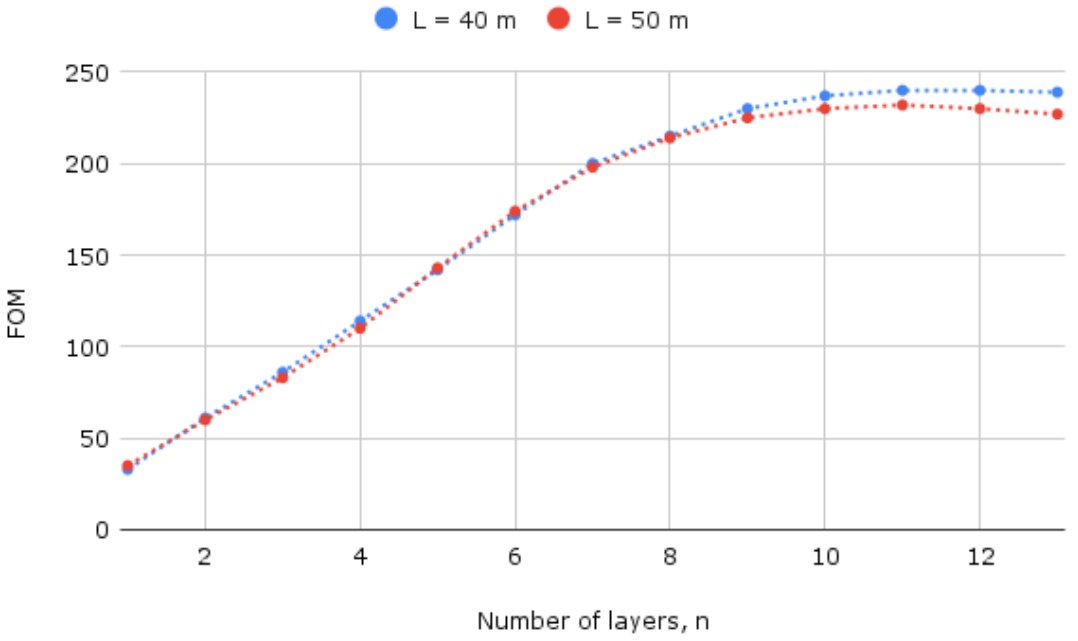

Figure 13: FOM variation with different number n of nested mirrors for 2 asymmetric Wolter optical systems ($L_H = 10$ m, $f_s = 20$ m)

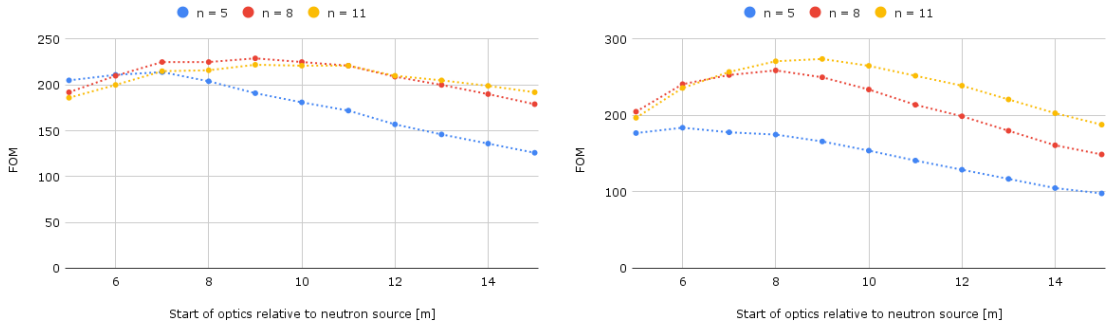

(a) $L = 40$ m, $L_H = 15$ m

(b) $L = 30$ m, $L_H = 10$ m

Figure 14: Variation in FOM value as the optics is designed to be positioned further away from the source

depending on the parameters of the system, and for the simulations in this section it already ranges from $n = 6$ to $n = 21$. Hence, in the case of asymmetric Wolter optics, it is important to check the exact value n_c for optimal FOM of each separate optical system that is simulated.

6.3 Varying f_s and the starting position of the optics ($f_s - L_H$)

As discussed in Section 6.1, Wolter optics have a preassigned position of maximum FOM, so shifting their starting point is only possible by constructing anew an optical system appropriate for that position. On Figure 14, the distance from the source to the intersection point ($f_s - L_H$) is varied, and the optimal FOM for each separate optics is recorded for two different mirror arrangements. The plots show that for all optics there is a peak in FOM for mirrors designed to have a starting position at about 9 m. While for the longer 40 m optic this peak is flattens out, the shorter 30 m optic has a more pronounced apex that encompasses a narrower range of mirror parameters. Hence, when longer mirrors are constructed, there is a greater allowance for selecting a starting position that returns a large FOM. In addition, adding more nested levels to the system also shifts the peak of the figure of merit to a greater distance away from the source. This is important, because the NNBAR will probably require the optics to start somewhere after the radiation blocking components encircling the source, and they are positioned at about 15 m from the source, far from the 9 m FOM peak.

Figure 14 a) shows that for a 40 meter optic with $L_H = 15$ m, an 11-layered system would not produce a larger FOM than a stack of 8 mirrors. This suggests that the excess material needed for constructing larger optics might be compensated by the smaller number of nested mirrors that the optics would require. However, Figure 14 b) shows that shorter optics might be able to outperform longer ones, as the overall FOM for the 30 m optic is larger than that for the 40 m optic. This is similar to the results obtained in the previous section: even though longer optics will reflect more neutrons, they also provide a smaller time of flight of the neutrons. The point at which these two factors configuring in the FOM balance out is now investigated.

6.4 Varying L_H and L

The exact length L_c at which the optics become less efficient is influenced by the ratio of L_H to L_E as shown on Figures 16 and 17. Varying first the hyperbolic length L_H, and then the total length L of the optics, the two mechanisms for changing the ratio of L_H to L_E are investigated. The simulations are run for three set-ups with a different number of nested levels: $n = 5$, $n = 8$ and $n = 11$. The length f_s is also varied in the first simulation (Figure 16), so that the starting

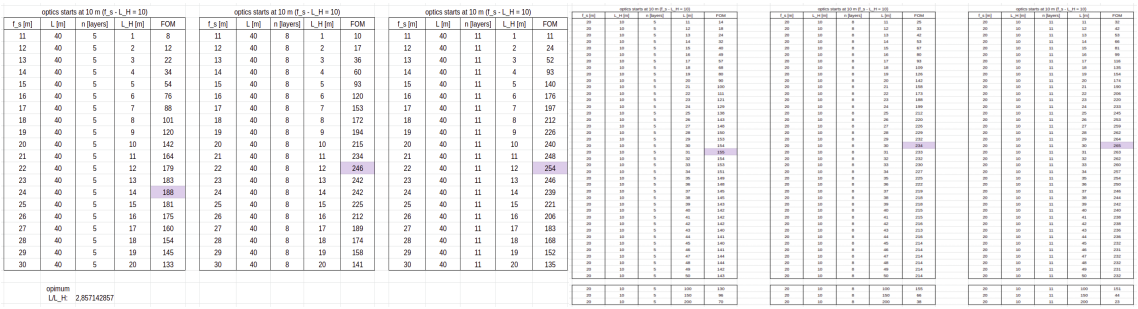

optics starts at 10 m (f_s - L_H = 10)

f_s [m]	L [m]	n [layers]	L_H [m]	FOM
11	40	5	1	8
12	40	5	2	12
13	40	5	3	22
14	40	5	4	34
15	40	5	5	54
16	40	5	6	76
17	40	5	7	88
18	40	5	8	101
19	40	5	9	120
20	40	5	10	142
21	40	5	11	164
22	40	5	12	179
23	40	5	13	183
24	40	5	14	188
25	40	5	15	181
26	40	5	16	175
27	40	5	17	160
28	40	5	18	154
29	40	5	19	145
30	40	5	20	133

optimum
L/L_H: 2.857142857

optics starts at 10 m (f_s - L_H = 10)

f_s [m]	L [m]	n [layers]	L_H [m]	FOM
11	40	8	1	10
12	40	8	2	17
13	40	8	3	36
14	40	8	4	60
15	40	8	5	93
16	40	8	6	120
17	40	8	7	153
18	40	8	8	172
19	40	8	9	194
20	40	8	10	215
21	40	8	11	234
22	40	8	12	246
23	40	8	13	242
24	40	8	14	242
25	40	8	15	225
26	40	8	16	212
27	40	8	17	189
28	40	8	18	174
29	40	8	19	159
30	40	8	20	141

optics starts at 10 m (f_s - L_H = 10)

f_s [m]	L [m]	n [layers]	L_H [m]	FOM
11	40	11	1	11
12	40	11	2	24
13	40	11	3	52
14	40	11	4	93
15	40	11	5	140
16	40	11	6	176
17	40	11	7	197
18	40	11	8	212
19	40	11	9	226
20	40	11	10	240
21	40	11	11	248
22	40	11	12	254
23	40	11	13	246
24	40	11	14	239
25	40	11	15	221
26	40	11	16	206
27	40	11	17	183
28	40	11	18	168
29	40	11	19	152
30	40	11	20	135

(a) Table 1.1: FOM values as a function of L_H for different number of nested mirrors

(b) Table 1.2: FOM values as a function of L for different number of nested mirrors

point of the optics ($f_s - L_H$) is fixed to 10 m. The total length L in this trial is 40 m.

In the second simulation, for f_s of 20 m, and $L_H = 10$ m the optics again are designed to have an optimal position 10 m away from the source. The raw data from these simulations is provided in Tables 1.1 and 1.2.

In both Figures 16 and 17, there is a peak of the FOM values at a certain ratio of $\frac{L_H}{L_E}$. For all scenarios that are simulated, this peak occurs roughly when $\frac{L_H}{L} = \frac{1}{3}$. Hence, we have

$$\frac{L_H}{L} = \frac{L_H}{L_H + L_E} = \frac{1}{3} \tag{60}$$

So,

$$L_E = 2L_H \tag{61}$$

This is not a strict requirement - even for the few set-ups that are simulated, the ratio of L_H to L varies from 2.8 to 3.1, and is not equal exactly to 3. However, equation 62 is still a very good approximation for the scenarios relevant to the NNBAR.

If the value of L_H is known, then Figure 17 shows that overshooting a bit the value of L that returns an optimum FOM does not lead to a very significant decrease in the figure of merit. In fact, after the maximum FOM is reached, values start to decline very slowly as L increases. On the opposite side of the curve, however, when the maximum FOM is still not achieved, adding longer elliptical sections (increasing L) has greater influence on the figure of merit. It is therefore, a much better strategy to overshoot for L_E (and L), then to undershoot when setting these parameters.

If, however, we decide to settle on a value for L, instead of inputting one for L_H, the FOM values rise much more steeply as the correct $\frac{L_H}{L_E}$ ratio is approached (see Figure 16). It is therefore harder and less efficient to approximate the hyperbolic lengths to ones that would produce an optimal FOM. Inputting L_H, and striving to find the best corresponding L value, is a far better alternative to inputting L and searching for the optimal L_H.

The first simulation also displays a shift of the optimal FOM values toward positions of smaller L_H as more nested levels are added. This is reminiscent of the observations made in section 6.2, where symmetric optics of shorter length L needed more nested levels to reach their optimal figure of merit. In both cases, as the total length L of the optics ($L = L_H + L_E$) decreases, more nested mirrors have to be added to reach the saturation of FOM that was observed on Figure 12.

Additionally, for both systems simulated in this section, the FOM value increases as more nested levels are added. The difference in FOM between 5 and 8 nested levels is larger than that

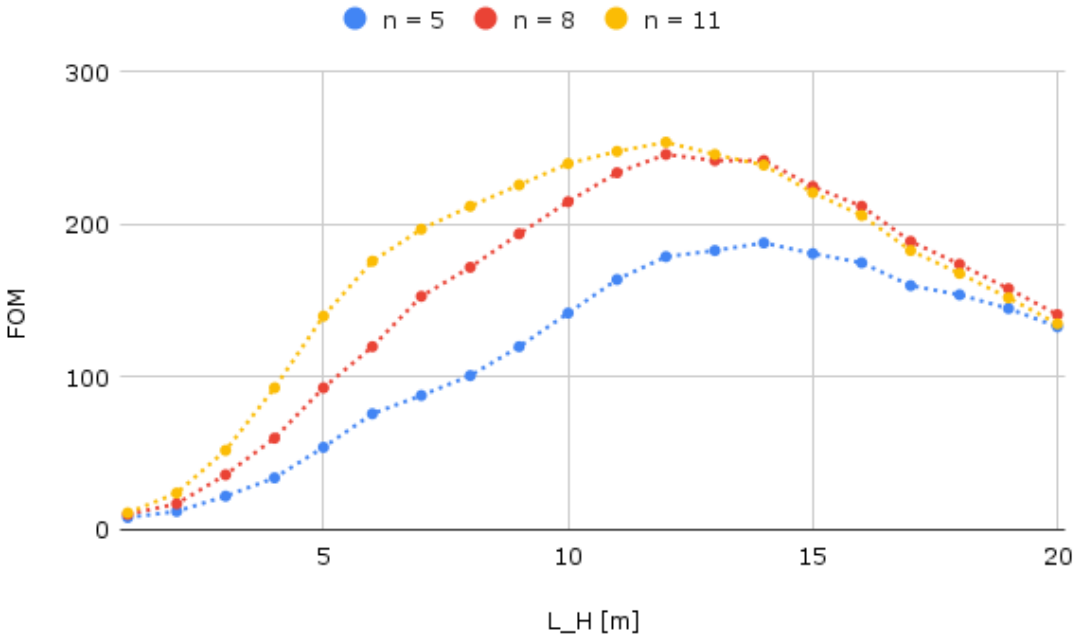

Figure 16: FOM values as a function of L_H for different number of nested mirrors

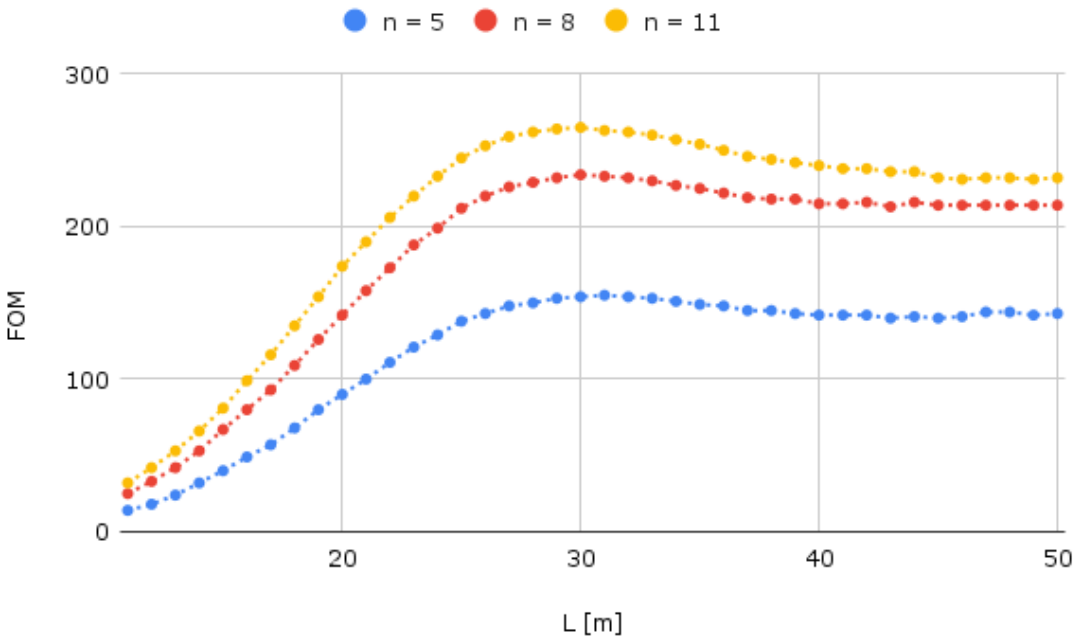

Figure 17: FOM values as a function of L for different number of nested mirrors

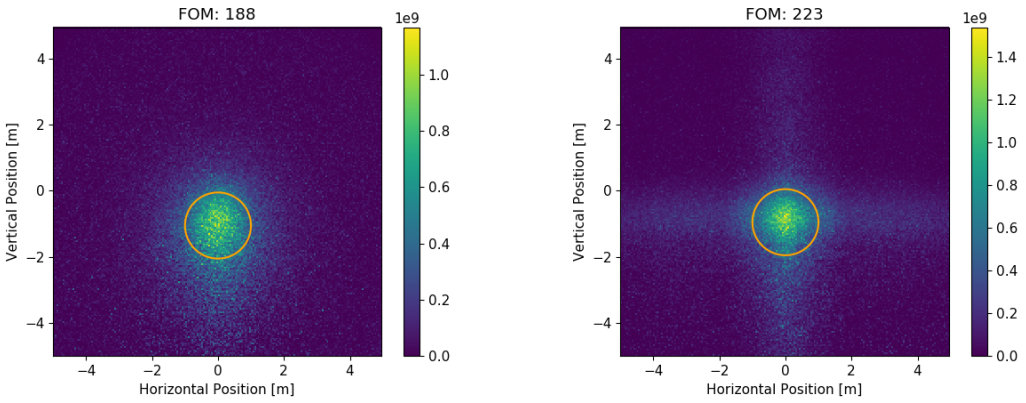

(a) FOM for a 40 m elliptical guide

(b) FOM for 40 m Wolter optics of $n = 11$

Figure 18: FOM comparison of an elliptical guide and Wolter optics

between 8 and 11 levels, which can be expected, as the optics must be approaching its FOM plateau by that point.

6.5 Comparison with an Elliptical Guide

To make a comparison between the efficacy of standard neutron guides and the more exotic Wolter arrangements of nested optics for the NNBAR experiment, we construct a guide of length 40 m and place it at $z_{start} = 10m$. From the previous sections, it can be estimated that an optics of a comparable length $L = 40$ m will perform best when $\frac{L_H}{L} = \frac{1}{3} = \frac{10}{30}$. Reading from Table 1.1, the optimal FOM for a 40 m optic with 11 nested levels positioned at $z_{start} = 10m$ is be achieved when $L_H = 12$ m. This FOM is over 220 (Figure 18 a)), while the elliptical guide only produces a FOM of 188 (Figure 18 b)). Hence, it is possible to construct Wolter optics that are more efficient to the purposes of the NNBAR experiment than elliptical guides.

7 Conclusion

Even though Wolter optics could produce better results for the NNBAR experiment than elliptical guides, they still rarely achieve the figures of merit that are required. A FOM of 300 was not reached even once for the optics that were simulated, with the largest FOM achieved being 274, at parameters $L = 30$ m, $L_H = 10$ m, $f_s = 19$ m and $z_{start} = 9$ m (see Figure 14 b)). It is probably possible to construct an optic that returns an FOM of 300 or maybe even the desired 333, but the author is sceptical about whether a higher figure of merit could be reached with Wolter optics.

Therefore, Wolter optics might provide a feasible solution to the NNBAR neutron transport problem, but it is also important to investigate other options for that experiment. For instance, it is possible that purely elliptical optics, such as the ones suggested by Oliver Zimmer [10], provide better figures of merit than Wolter optics. When only elliptical mirrors are used, this reduces the absorption rate by the reflector, since only two reflections are be required to direct the beam, as opposed to the four reflections from a double planar Wolter optic. However, this increase in flux comes at the expense of a worse focusing, as the ellipses produce a more blurred image than Wolter optics. It is important, therefore, to also simulate elliptical mirrors with the exact parameters of the NNBAR system, so that the better optical system can be chosen.

Even if nested Wolter optics do not end up being used at the NNBAR experiment, they are still very promising venue of exploration for neutron transport. The FOM plots on Figure 18 show that Wolter optics have a much better focusing ability than the conventional guides. Hence, they can be useful for neutron transport to small samples where precision in the width of the transported beam is required. In addition, when the time of flight reset was turned off by accident in the FOM calculations, the simulations achieved stunning FOM values that could reach more than 800. This suggests that the Wolter optics are really good at transporting a large number N of neutrons, so they can be useful in experiments that require an in-beam transport of a large flux.

References

[1] Pareschi G, Spiga D, Pelliciari C. X-ray Telescopes Based on Wolter-I Optics. In: The WSPC Handbook of Astronomical Instrumentation: Volume 4: X-Ray Astronomical Instrumentation. World Scientific; 2021. p. 3-31.

[2] VanSpeybroeck L, Chase R. Design parameters of paraboloid-hyperboloid telescopes for X-ray astronomy. Applied Optics. 1972;11(2):440-5.

[3] Thompson PL, Harvey JE. Aplanatic Wolter Type-I telescope design: is there a practical advantage? In: X-Ray Optics, Instruments, and Missions. vol. 3444. SPIE; 1998. p. 526-42.

[4] Hussey DS, Abir M, Cook JC, Jacobson DL, LaManna J, Kilaru K, et al. Design of a neutron microscope based on Wolter mirrors. Nuclear Instruments and Methods in Physics Research Section A: Accelerators, Spectrometers, Detectors and Associated Equipment. 2021;987:164813.

[5] Addazi A, Anderson K, Ansell S, Babu K, Barrow J, Baxter D, et al. New high-sensitivity searches for neutrons converting into antineutrons and/or sterile neutrons at the HIBEAM/NNBAR experiment at the European Spallation Source. Journal of Physics G: Nuclear and Particle Physics. 2021;48(7):070501.

[6] Santoro V, Andersen KH, DiJulio D, Klinkby EB, Miller T, Milstead D, et al. Development of high intensity neutron source at the European Spallation Source. Journal of Neutron Research. 2020;22(2-3):209-19.

[7] Baldo-Ceolin M, Benetti P, Bitter T, Bobisut F, Calligarich E, Dolfini R, et al. A new experimental limit on neutron-antineutron oscillations. Zeitschrift für Physik C Particles and Fields. 1994;63(3):409-16.

[8] Frost M. Observation of Baryon Number Violation via Cold Neutron Sources. 2019.

[9] Khaykovich B, Gubarev M, Bagdasarova Y, Ramsey B, Moncton D. From x-ray telescopes to neutron scattering: Using axisymmetric mirrors to focus a neutron beam. Nuclear Instruments and Methods in Physics Research Section A: Accelerators, Spectrometers, Detectors and Associated Equipment. 2011;631(1):98-104.

[10] Zimmer O. Multi-mirror imaging optics for low-loss transport of divergent neutron beams and tailored wavelength spectra. arXiv preprint arXiv:161107353. 2016.

[11] Bagdasarova YS. Wolter mirror microscope: Novel neutron focussing and imaging optic. Massachusetts Institute of Technology; 2010.

[12] Howells MR. Mirrors for synchrotron-radiation beamlines. In: New Directions in Research with Third-Generation Soft X-Ray Synchrotron Radiation Sources. Springer; 1994. p. 359-85.

[13] Berendonk S. Proving the reflective property of an ellipse. Mathematics Magazine. 2014;87(4):276-9.

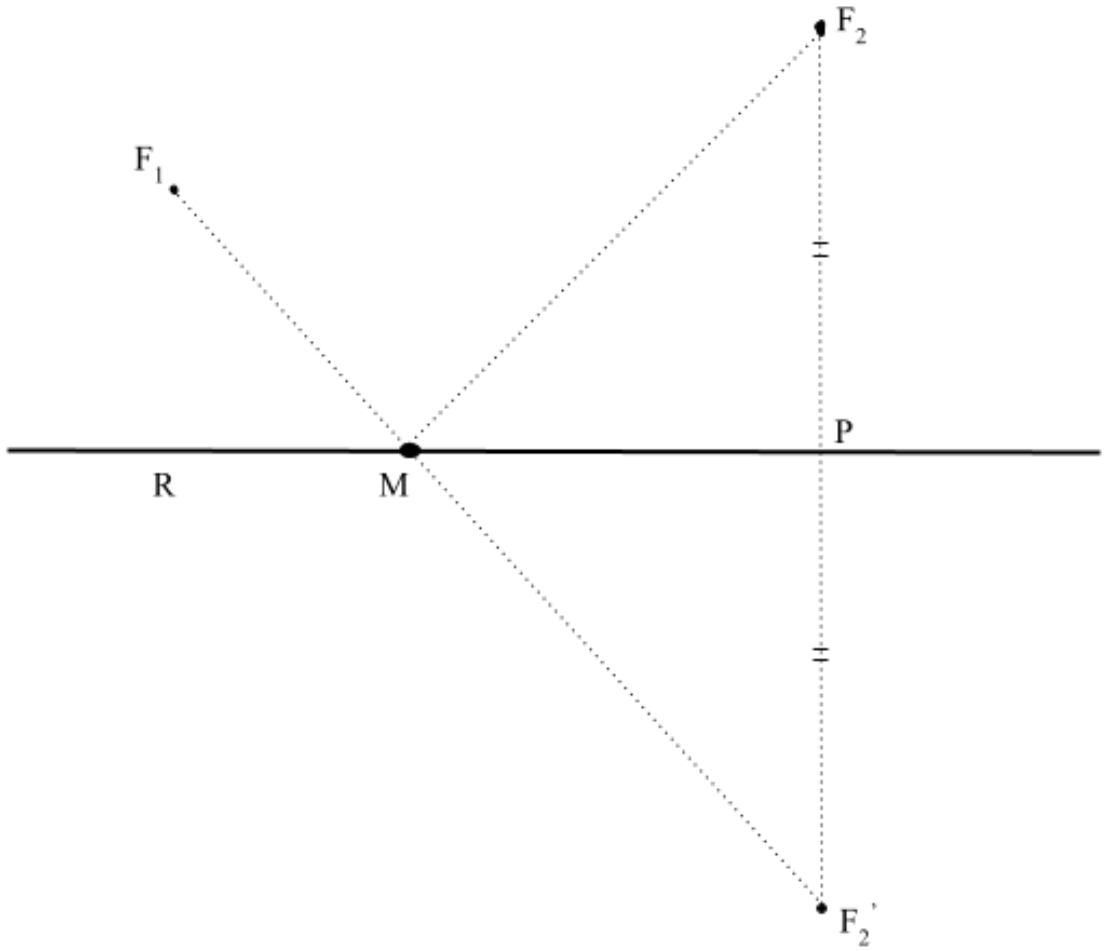

Figure 19: Proof of Reflection Property of Ellipse

8 Appendix I: Reflection by Conic Sections

8.1 Ellipse

It was stated in section 3.3.1 that a ray passing through one of the focal points of an ellipse and reflecting off its surface heads toward the other focus. A two-step sketch of the proof is provided here (also see [13]).

1) Firstly, consider two points F_1 and F_2 that lie on the same side of a line as shown on Figure 19. We want to find the shortest distance between F_1 and F_2 that touches the line. To do this, we reflect the point F_2 across the line to F_2'. Assuming that the shortest distance passes through some point M on the line, we notice that $\angle F_2MP = \angle F_2'MP$ and $F_2M = F_2'M$. Hence, $F_1M + MF_2 = F_1M + MF_2'$, so finding the shortest distance between F_1 and F_2 that touches the line is equivalent to finding the shortest distance from point F_1 to point F_2'. But we know that the shortest distance between two points is just the straight line connecting them. Therefore, point M must lie on the line F_1F_2', so $\angle F_1MR = \angle F_2'MP = \angle F_2MP$. Hence, the shortest distance between two points that passes through a given line is actually a reflection off the surface of the line.

2) We now use what we found in step 1) to prove that if F_1 and F_2 are the two foci of an ellipse,

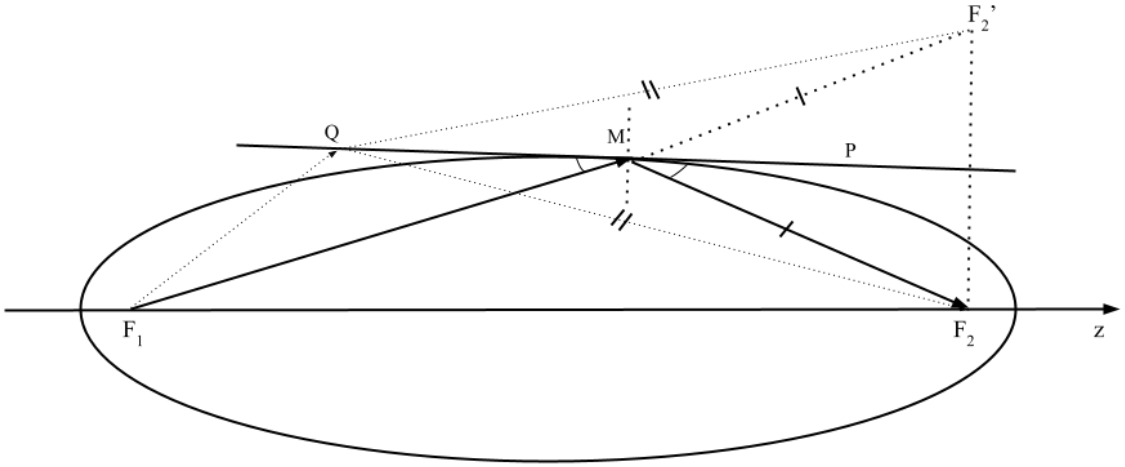

Figure 20: Proof of Reflection Property of Ellipse

then point M would lie on its surface. Firstly, we draw on Figure 20 an ellipse with its two foci and choose an arbitrary point M on its surface. We extend F_1M by MF_2' such that $MF_2' = MF_2$. We now draw a line l through M that bisects the line F_2F_2'. Hence F_2' is a reflection of F_2 about the line l. We will show that this line has to be the tangent to the ellipse at point M.

We assume toward a contradiction that l is not tangent to the ellipse at point M. Hence, l has to touch the ellipse a second time. We call the point of intersection Q. Now we use the defining property of an ellipse - that it is the locus of points for which the sum of the distances to its two foci is constant. Hence, we have that $F_1Q + QF_2 = F_1M + MF_2 = F_1M + MF_2' = F_1F_2'$. But from triangle F_1QF_2' we know that this can not be true - the sum of two of sides of a triangle always has to be greater than the length of the other side. Hence, we have arrived at a contradiction, and l must be the tangent line to the ellipse. Therefore, using 1), we know that the angles $\angle F_1MQ = \angle F_2MP$ are the glancing angles of incidence and reflection at point M on the surface of the ellipse, so indeed the ray $\overrightarrow{MF_2}$ is a reflection of the ray $\overrightarrow{F_1M}$. Since M was an arbitrary point on the ellipse, it is true that more generally any ray incoming from one of the foci of an ellipse reflects off its surface towards the other focus.

8.2 Hyperbola

A hyperbola has a very similar property - the reflection of a ray coming from one of its foci appears to be originating at its other focus. To prove this, we first draw an arbitrary ray starting at F_1 on Figure 21 that intersects the hyperbola at point M. Then, we choose a point Q on F_1M such that $QM = MF_2$. We can see that $F_1Q = F_1M$ - $QM = F_1M$ - MF_2. This is important because a hyperbola is defined as the locus of points for which the difference of the distances to the two foci is constant. We now know that this constant is equal to F_1Q.

Now we call L the midpoint of MF_2. Triangles LMQ and F_2ML are equivalent, so the angles $\angle LMQ$ and $\angle LMF_2$ are equal. Similar to the ellipse case, we now only need to prove that LM lies on the tangent to the hyperbola at point M to conclude that the reflective property is satisfied. To do this, we once again assume towards a contradiction the contrary.

If LM is not lying on a tangent line to the ellipse, then it must intersect it one more time. We call this second point of intersection P. Noticing that QP = PF_2, we have $F_1Q + QP > PF_1$, so $F_1Q > PF_1 - PF_2$. But this means that $PF_1 - PF_2 \neq F_1Q$, so the point P can not lie on the hyperbola. Thus, we have a contradiction, and the line MP must be part of the tangent to the

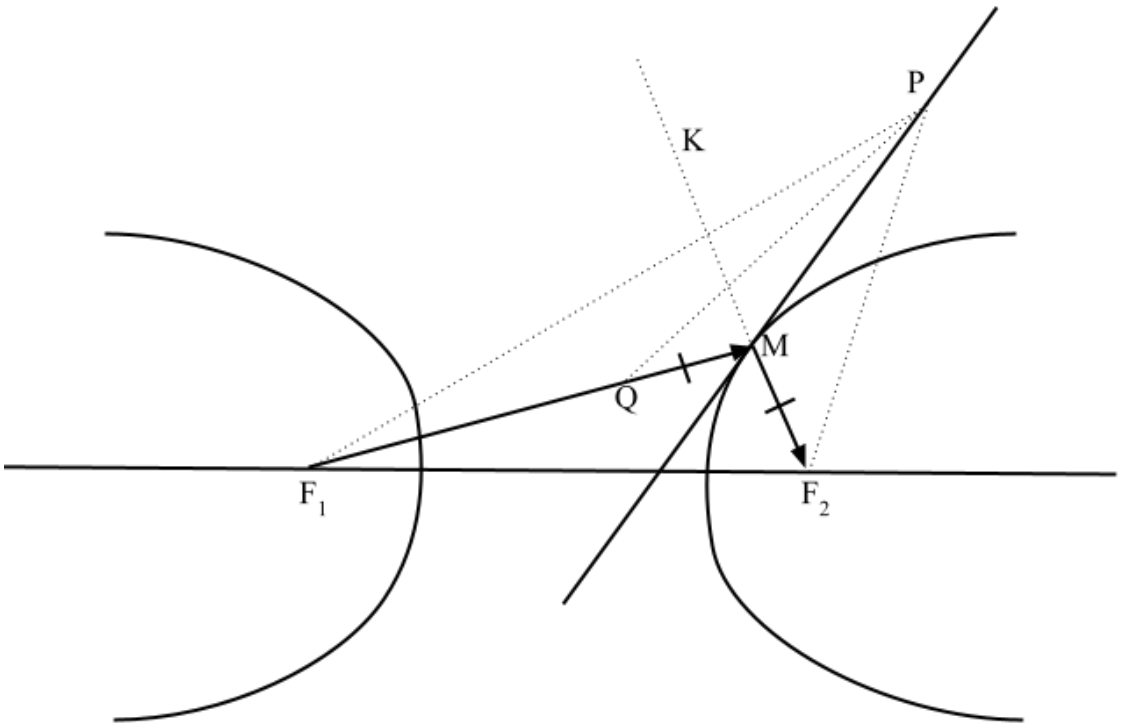

Figure 21: Proof of Reflection Property of Ellipse

ellipse at point M. If we extend that tangent as on Figure 21, we get that $\angle LMF_2 = \angle PMK$ (P not on the surface of the hyperbola, as proven). But we have already found that $\angle LMQ = \angle LMF_2$, so we have that $\angle LMQ = \angle PMK$. Hence $\overrightarrow{MK}$ is a reflection of ray $\overrightarrow{F_1M}$. But MK is an extension of the line F_2M, so indeed it appears that the reflection of $\overrightarrow{F_1M}$ coming from the first focal point of the hyperbola originates from the other focus (F_2). Because M was an arbitrary point, we can generalise this property to all points on the surface of the hyperbola.

9 Appendix II: Ellipse Approximation

In section 3.1 an approximation was made to establish the arrays of heights at the intersection point. It argued that for the bulk of the hyperbola surface, the ratios between the heights of two consecutive hyperbola layers are preserved at any point on the z-axis. A similar argument applies for an ellipse.

On Figure 22,

$$\frac{y_{n-1,E}(z)}{y_{n,E}(z)} - \frac{r_{n-1}}{r_n} \tag{62}$$

is plotted for the range of z values covering the surface of the ellipses.

For z-values to the left of the intersection point ($z < -f_s$), the maximum value of the ratio difference is 0.0015, so $\frac{r_{n-1,E}}{r_{n,E}}$ can be approximated to $\frac{y_{n-1,E}(z)}{y_{n,E}(z)}$ for the coordinates that define the ellipse portion of the Wolter set-up. As with the hyperbolas, the approximation becomes better going inwards into the nested mirror system. In addition, the mid-sections of the different

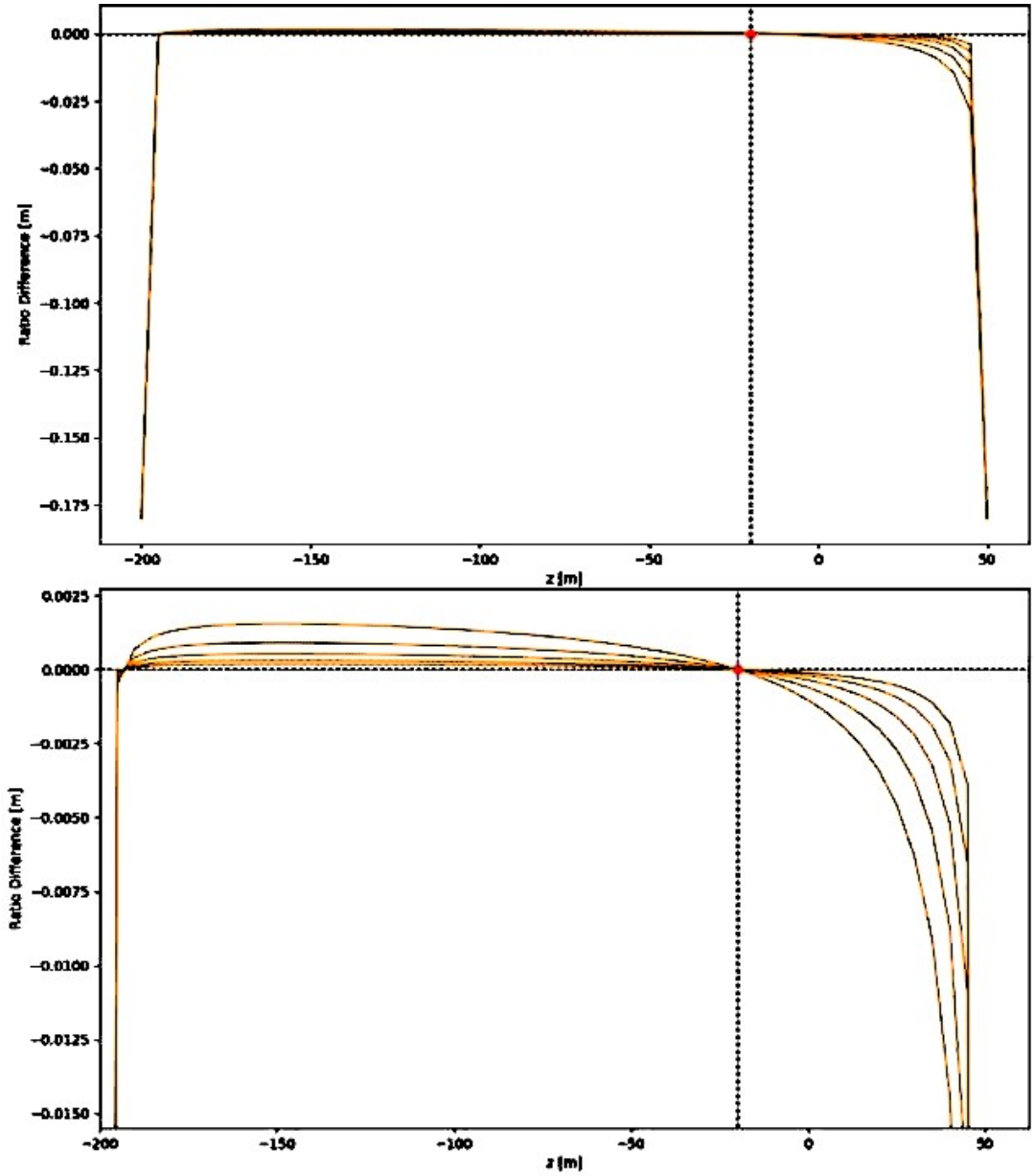

Figure 22: Differences between ratios $\frac{y_{n-1,E}(z)}{y_{n,E}(z)}$ and $\frac{r_{n-1}}{r_n}$ for different z-values of a system of six nested levels with a zoom-in into the region $2c_0, H > z > -f$. The top line on the left corresponds to the difference for levels $n = 0$ and $n = 1$.

ellipses are also covered by this slice of the z-axis, so it might be relevant for the construction of nested elliptical optics.

10 Appendix III: Navigating Through the Code

10.1 final_half_axes

Starting with the mathematical foundations outlined in sections 1-4, the notebook final_half_axes creates arrays of semi-minor ellipse and hyperbola axes from given r_0, f_i, f_s, L_H, L and n. This notebook is also able to visualise the system (via the function wolter_plot()) and to create the plots of the appropriate intersection heights for nesting the mirrors.

10.2 mono_planar_off_file_creation

This notebook creates OFF files for horizontal monoplanar nested systems. The optics need to be rotated externally after being imported into McStas to get a vertical arrangement.

The coordinates() function assigns appropriate y-values to each z coordinate and splits the x-axis into an arbitrary number of segments. These coordinates are then written down in the off file by the function monoplanarOFF. The coordinates are first ordered according to the nested level they belong to. For each nested level, first the coordinates of the upper mirror are encoded, then those of the lower mirror. For each mirror, coordinates are ordered starting from the front right corner of the optics and going along the z-axis for each fixed x coordinate. The code ensures that the coordinates of the last x-value and those at the end of each line z-positions are not used to begin writing a new face, as there would be no coordinates following them that could be used to finish the face.

10.3 double_planar_off_file_creation and simplified_double_planar

The double planar arrangement consists of two monoplanar systems at right angles to each other. The monoplanar optics are created in the same manner as before, but the doubleplanarOFF() function exchanges the x and y coordinates of one of them, so that it gets rotated.

The double_planar_off_file_creation notebook produces a file with more faces, as it also splits the optics along the x-axis (x = -2, x = -1.75, x = 1.5, etc). This is why this notebook is heavier than simplified_double_planar where only the z and y axes are segmented and panels go along the whole x dimension (x = -2 to x = 2 for NNBAR). The extra panels should not make much difference to the results, so it is recommended to use the simplified version to get faster simulations.

10.4 NNBAR_TestEnvironment_Wolter

This notebook was created by Richard Wagner. It can be used to test a single OFF file as an optics arrangement for the NNBAR experiment. The mirrors should be set at (0, -0.273, 0) in the code, so that they start at the correct position for the Wolter optics. The y-coordinate is set to -0.273 to account for the specifications of the source - there is more neutron flux below the optical axis than above it.

10.5 fast_NNBAR

This notebook is almost identical to the previous one, but it allows you to test an OFF file by placing the optics sequentially at multiple coordinates. As was found (and expected from theory), the Wolter optics has only one proper position coordinate, as it is designed for a specific distance from source to the optics ($f_s - L_H$). Hence, the reflector has to be set at z = 0, as

previously suggested, since the OFF file already contains the appropriate start point of the optics. It can checked artificially by opening the OFF file and examining the first z-coordinate that is present there or it can be calculated as $f_s - L_H$. Unless one wants to replicate the results from tables 1 and 2, and verify that Wolter optics focus well only when they are positioned correctly, one would not find much use in this notebook.